INTERNATIONAL JOURNAL FOR NUMERICAL AND ANALYTICAL METHODS IN GEOMECHANICS
Int. J. Numer. Anal. Meth. Geomech. 2012; **36**:249–271
Published online 5 January 2011 in Wiley Online Library (wileyonlinelibrary.com). DOI: 10.1002/nag.1004

Approximate model for blunt objects indenting cohesive-frictional materials

J. P. Hambleton*, † and A. Drescher

Department of Civil Engineering, University of Minnesota, 500 Pillsbury Drive SE, Minneapolis, MN 55455, U.S.A.

SUMMARY

An approximate two-dimensional model for indentation of blunt objects into various types of rigid-perfectly plastic cohesive-frictional material is derived. Particular emphasis is placed on considering indentation as a process involving evolution of the boundary of material displaced by the indenter. Force–penetration relationships are obtained by an incremental approach utilizing key kinematic and static information from indentation of a flat punch. Albeit approximate, the proposed model applies to arbitrary indenter geometry and weightless or ponderable cohesive-frictional materials exhibiting associated or non-associated plastic flow. Two specific indenter geometries, the cylinder and blunt wedge, are explored in detail. Favorable agreement is found between the analytic results and those obtained using the finite element method (FEM). For both the wedge and cylinder, it is further shown that accurate analytic expressions relating indentation force explicitly to penetration can be derived. In the case of the wedge and weightless material, predictions of indentation force obtained from the derived expressions are very close to those computed from implicit equations available in the literature. Copyright © 2011 John Wiley & Sons, Ltd.

Received 23 March 2010; Revised 28 October 2010; Accepted 10 November 2010

KEY WORDS: indentation; rigid-plastic; cohesive-frictional; cylinder; wedge; finite element method

1. INTRODUCTION

Penetration of a rigid object into plastically deforming material commonly occurs in a number of applications. Tests for evaluating strength of metallic materials, for example, are usually based on indentation of spheres, cones, and pyramids [1]. Likewise, indentation of conical and non-conical objects into soils is a well-recognized practical methodology for determining *in situ* properties [2]. Indentation also represents a fundamental mode of operation in soil–machine interaction (SMI), where components of agricultural and earth-moving machinery of various types penetrate the soil [3, 4]. Additional areas where penetration of an object may be of interest are sediment–object interaction in marine environments and processing of bulk materials.

This paper is concerned with theoretically modeling the process of quasi-static normal indentation of blunt, two-dimensional (plane strain) objects into rigid-perfectly plastic cohesive-frictional material. Concentration on the process rather than a particular state necessitates consideration of the evolving contact interface between the indenter and material as well as the evolution of the lips forming next to the indenter, which possess a geometry that is unknown beforehand. Accordingly, the problem belongs to the class of unknown boundary type for which solutions may be non-unique [5, 6]. The term 'blunt' implies that the ratio of penetration depth to contact length

*Correspondence to: J. P. Hambleton, Department of Civil Engineering, University of Minnesota, 500 Pillsbury Drive SE, Minneapolis, MN 55455, U.S.A.
†E-mail: hamb0025@umn.edu

is relatively small. Normal indentation is directly involved in many instances in the applications indicated above and may be used to approximate oblique and/or rotational indentation provided the inclination of the object's trajectory from the surface normal is limited and the object's rotational velocity is small.

An example of two-dimensional object indentation, which is also the problem considered most in the literature, is that of wedge indentation into perfectly plastic cohesive or frictional material. Solutions for a weightless material based on the method of characteristics (slip lines) can be attributed to Hill *et al.* [7], Shield [8], Grunzweig *et al.* [9], Haddow [10] Bai and Dodd [11], and Tordesillas and Shi [12]. Drescher *et al.* [13] included the effect of weight in their numerical slip-line calculations, whereas Drescher and Michalowski [14] incorporated weight within the framework of the kinematic method of limit analysis. Some of these works considered flow rules other than classical associated flow. Experimental results can be found in Drescher *et al.* [13] and Butterfield and Andrawes [15], and a discussion of kinematical requirements for wedge indentation in cohesive-frictional materials with and without weight is provided by Butterfield [16]. Exploratory results on cylinder indentation into soils can be found in the authors' earlier work [17].

Previous works on normal indentation are limited in several respects. First, most of these works do not consider the effect of material weight. By excluding material weight, indentation into purely frictional material does not require any force, and this is physically incorrect when gravity is present. Second, the solutions do not furnish explicit formulae amenable for usage in practice. Finally, each previous study focuses on one particular indenter geometry (e.g. wedge), and to the authors' knowledge, no universal and efficient methodology applicable to a variety of geometries exists.

In this paper, a generic approach for determining the force–penetration relationship for a blunt object indenting cohesive-frictional material is presented. This model accommodates material weight and leads to approximate analytic formulae for indentation force for virtually any blunt indenter. The proposed analytic method is premised on constructing the total deformation induced by an indenter as a summation of incremental responses, where the incremental response can be evaluated from solutions to the fundamental plasticity problem of a flat punch pressed into a straight or trapezoidal surface (truncated wedge). The corresponding force acting on the indenter is obtained from integrating the average vertical stresses at the punch–material interface.

The punch problem was also used by Hambleton and Drescher [17] as the basis for approximate analysis of cylinder indentation. The present model is significantly different, however, in that it incorporates the evolution of material lips forming during indentation, thereby capturing the actual contact length. In the earlier work, displaced material was simply replaced by surcharge, which had negligible influence on the resulting force–penetration curves.

The material model assumed in the analysis is rigid-perfectly plastic, with the linear Mohr–Coulomb yield condition that is characterized by two material constants: friction angle ϕ and cohesion c. The unit weight of the material is denoted γ. The flow rules governing the deformation are considered to be coaxial associated or non-coaxial with dilation angle ψ.

For assessing the accuracy of the solutions obtained, the results of elastic–plastic computations using the finite element method (FEM) are also presented, where high elastic modulus emulated the response of the rigid-perfectly plastic model.

2. APPROXIMATE MODEL

The model presented below aims at relating the vertical indentation force Q to the penetration δ defined as the vertical distance between the indenter's lowermost point and the undisturbed material surface (Figure 1). The geometry of the rigid, symmetric indenter is specified through the function $f(x)$, where $f(x)$ is strictly increasing and defines curve in the $x-y$ coordinate system shown in Figure 1. The origin of the $x-y$ system is coincident with the lowermost point of the indenter and translates into the negative y-direction as penetration δ increases. Material is displaced upward on either side of the indenter, forming material lips that intersect the indenter surface at height l above the undisturbed surface. The indenter contacts the deformed surface over a horizontal distance h.

DOI: 10.1002/nag

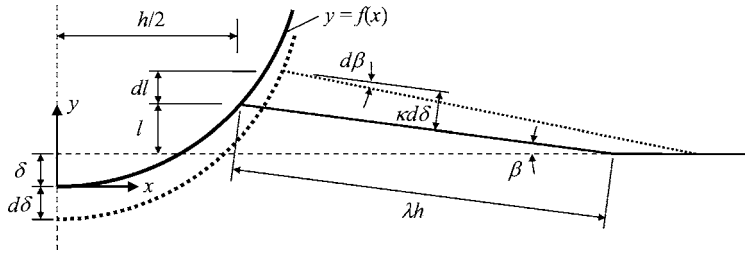

Figure 1. Indentation of a blunt, symmetric object.

The basic postulate regarding the deformation induced by the indenter is that the material lips adjacent to the indenter are straight, with angle of inclination to the horizontal denoted β. As shown in Figure 1, the length of either lip is given by λh, where λ is in general a non-constant multiplier. When the process of indentation is assumed to be geometrically self-similar, β and λ are necessarily constants; however, self-similarity is not imposed *a priori* in the approximate model. Self-similarity in the case of wedge indentation was considered by Hill *et al.* [7], Shield [8], Drescher and Michalowski [14], and Tordesillas and Shi [12] among others. During an increment of penetration $\mathrm{d}\delta$, the lip surface moves a distance $\kappa\mathrm{d}\delta$ along the surface normal at the point where the lip surface contacts the indenter (Figure 1), where κ is another multiplier. The multipliers λ and κ depend on the parameters in the yield condition and the flow rule. However, it is recognized that λ and κ may not be independent.

An additional simplifying assumption made throughout the remainder of the paper is that angle β is small ($\cos\beta \approx 1, \sin\beta \approx \beta$). Angle β can then be related to l and h by

$$\beta = \frac{l}{\lambda h} \tag{1}$$

The equation governing the evolution of the lips in the course of indentation is derived by examining the kinematics at the point where the lip meets the indenter surface. As shown in Figure 2, an infinitesimal change in indenter displacement, $\mathrm{d}\delta$, is geometrically related to the change in lip height, $\mathrm{d}l$. Line segments AC and CD have lengths given by

$$\overline{AC} = \mathrm{d}\delta\cot\alpha + \mathrm{d}l\cot\alpha - \mathrm{d}l\tan\beta \tag{2}$$

$$\overline{CD} = \kappa\mathrm{d}\delta - \mathrm{d}l\sec\beta \tag{3}$$

In (2), α is the angle between the tangent to the indenter and the horizontal at the point where the deformed material boundary meets the indenter surface (at height l above the undisturbed surface), and it is related to $f'(x) = \mathrm{d}f(x)/\mathrm{d}x$ through

$$\tan\alpha = f'(h/2) \tag{4}$$

Contact length h in (4) is related to δ and l through

$$\delta + l = f(h/2) \tag{5}$$

Since $\sin\beta = \overline{CD}/\overline{AC}$ (Figure 2), one may deduce the following relationship between $\mathrm{d}l$ and $\mathrm{d}\delta$:

$$\sin\beta = \tan\alpha\frac{\kappa\mathrm{d}\delta - \mathrm{d}l\sec\beta}{\mathrm{d}\delta + \mathrm{d}l - \mathrm{d}l\tan\alpha\tan\beta} \tag{6}$$

Combining Equations (1) and (6) and utilizing the small-β approximation gives, after some manipulation, the following ordinary differential equation:

$$\frac{\mathrm{d}l}{\mathrm{d}\delta} = \kappa - \frac{\kappa+1}{\dfrac{\lambda h}{l}\tan\alpha + 1} \tag{7}$$

DOI: 10.1002/nag

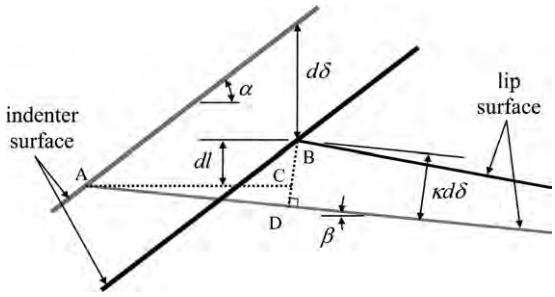

Figure 2. Incremental kinematics at point where deformed material boundary meets indenter surface.

Once $f(x)$, λ, and κ, are specified, Equation (7) may be solved, analytically or numerically, to determine l as a function of δ. It should be pointed out that λ, κ, h, and $\tan\alpha$ in general depend on δ and l, making (7) a non-trivial differential equation.

The magnitude of the vertical force Q is derived from the average normal traction q acting along the distance h

$$Q = qh \tag{8}$$

where both q and h in general change as functions of δ.

Finally, it is postulated that the traction q, as well as the multipliers λ and κ, may be assessed from results for the problem of a flat rigid punch of width h pressed into a flat or slightly sloping surface (truncated wedge) of plastically deforming material. The punch problem refers to incipient flow beneath and around a rigid punch and not to the process of continuous penetration. The process of indentation is thus modeled as a sequence of incipient problems, with the overall geometry changing from one increment to the next but the incremental variation being considered equivalent to the incipient flow problem. The solutions for this problem with weightless or ponderable material obeying associated and non-associated flow rules are presented in the following section.

3. PUNCH INDENTATION

3.1. Weightless material

For weightless cohesive-frictional materials obeying the (coaxial) associated flow rule ($\psi = \phi$), the two well-known solutions obtained by the method of characteristics are shown in Figure 3 [18]. On the left-hand side is the Prandtl-type solution referred to as the 'rough' punch solution, and on the right-hand side is the Hill-type solution applicable to a 'smooth' punch. Next to the punch, and next to the free boundary, the characteristics are straight, and in the transition zone one family is straight (fan) and the other forms log-spirals (circles for $\phi = 0$). In either case, the velocity and stress characteristics coincide and the free boundaries move uniformly. Also, multipliers λ and κ, which define the extent and incremental movement of the free boundaries, are given by analytic expressions. Multiplier κ derives from the ratio of the normal component of velocity of the free boundary next to the punch and the velocity of the punch, both determined from the hodograph (velocity plan).

For the Prandtl-type solution, which is physically more realistic than the Hill-type solution, the expressions for q, λ, and κ are

$$q = c\cot\phi\left[\tan^2\left(\frac{\pi}{4}+\frac{\phi}{2}\right)e^{(\pi-2\beta)\tan\phi}-1\right] \quad \text{for } \phi\neq 0, \quad q = c(2+\pi-2\beta) \quad \text{for } \phi = 0 \tag{9}$$

$$\lambda = \tan\left(\frac{\pi}{4}+\frac{\phi}{2}\right)e^{(\frac{\pi}{2}-\beta)\tan\phi} \quad \text{for } \phi\neq 0, \quad \lambda = 1 \quad \text{for } \phi = 0 \tag{10}$$

$$\kappa = \frac{1}{2}\tan\left(\frac{\pi}{4}+\frac{\phi}{2}\right)e^{(\frac{\pi}{2}-\beta)\tan\phi} \quad \text{for } \phi\neq 0, \quad \kappa = \frac{1}{2} \quad \text{for } \phi = 0 \tag{11}$$

DOI: 10.1002/nag

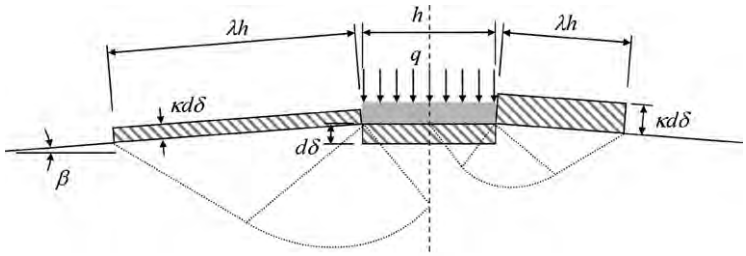

Figure 3. Indentation of punch on weightless material showing Prandtl-type mechanism (left-hand side) and Hill-type mechanism (right-hand side).

It may be noted that expressions for λ and κ differ only by a factor of one half. Equations (9)–(11) also apply to the Hill-type mechanism, with a factor of one half multiplying the expression for λ, and the factor of one half removed from the formulas for κ.

Experiments on soils clearly demonstrate that the associated flow rule predicts excessive dilation for granular soils, and for this reason alternative flow rules, including (coaxial) non-associated and non-coaxial flow rules (cf. [19]), have been utilized. While these alternative flow rules in most cases model the behavior of soils more accurately than the associated flow rule, they also complicate the analysis considerably. Namely, uniqueness and upper/lower bound theorems on collapse loads are not obtainable, and the collapse load can be affected by dilatancy, elastic properties, and loading history. For a thorough discussion on the influence of the flow rule, the reader is referred to the works of Vermeer and de Borst [20, 21], who analyzed a number of boundary value problems including the punch problem.

If the flow rule is coaxial non-associative ($\psi<\phi$), velocity characteristics do not coincide with those for stresses, and the region undergoing plastic deformation is smaller than with $\psi=\phi$ [22]. In the fan, both sets of velocity characteristics are curved. As a consequence, the velocity field becomes complex, and the free boundary does not move uniformly. More importantly, as shown by Drescher and Detournay [23] the solution based on the method of characteristics is thermodynamically inadmissible and has no physical value.

One possible means of accounting for non-associativity that preserves the simplicity of Prandtl- and Hill-type solutions [23] involves the use of reduced friction angle and cohesion given by

$$\tan\phi^* = \frac{\cos\psi\cos\phi}{1-\sin\psi\sin\phi}\tan\phi \tag{12}$$

$$c^* = \frac{\cos\psi\cos\phi}{1-\sin\psi\sin\phi}c \tag{13}$$

However, the new parameters ϕ^* and c^* cannot be used in the expressions for λ and κ because this would lead to overestimation of the global incremental volume increase. For example, the volume of material displaced along the free boundaries with $\psi=0$ and $\phi^*>0$ would not equal the volume displaced by the punch, and the incompressibility requirement would be violated.

The non-coincidence of stress and velocity characteristics in coaxial non-associated flow rules has been disputed on the basis of violating the concept of sliding along planes where the Mohr–Coulomb yield condition is satisfied, i.e. the stress characteristics or slip lines, as discussed by de Josselin de Jong [24], Spencer [25], and Mehrabadi and Cowin [26]. Enforcing the sliding concept leads to non-coaxiality of principal stresses and strain rates in some problems, an example being punch indentation [12, 25]. As the field of stress characteristics remains identical to that of the coaxial flow rule, the value of q and the extent of the deforming material defined by λ remain unchanged and are given by Equations (9) and (10), respectively, for the Prandtl-type solution.

DOI: 10.1002/nag

However, multiplier κ now assumes a different value given by

$$\kappa = \frac{1}{2} \frac{\cos\phi \cos\left(\frac{\pi}{4} + \frac{\phi}{2} - \psi\right)}{[\cos(\phi - \psi) - \sin\psi] \sin\left(\frac{\pi}{4} + \frac{\phi}{2}\right)} e^{-\tan(\phi - 2\psi)\left(\frac{\pi}{2} - \beta\right)} \tag{14}$$

For the Hill-type solution, the comments for the associated flow rule still apply. With $\psi = \phi$, Equation (14) is the same as (10), making (14) valid for all admissible values of ψ. Also, $\kappa = 1/(2\lambda)$ with $\psi = 0$ as required by incompressibility.

*3.2**3**Ponderable material*

For ponderable cohesive-frictional materials, where the method of characteristics still applies, the field of characteristics becomes very complex and must be determined numerically rather than analytically [27]. Accordingly, the tractions at the punch–material interface and the velocities at the free boundary are non-uniform regardless of whether the flow rule is coaxial associative or non-coaxial. This precludes the possibility of arriving at rigorous analytic expressions for q, λ, and κ.

An approximation often used in practical applications is the formula for q originally proposed by Terzaghi [28]

$$q = cN_c + \tfrac{1}{2}\gamma h N_\gamma \tag{15}$$

Equation (15) is based on the field of stress characteristics for a weightless material, with the effect of weight superimposed. This would also imply that λ and κ are the same as for a weightless material, a characteristic that is not supported by numerical calculations [27]. While the factor N_c is identically equal to q/c given by Equation (9), proper values of the factor N_γ have been debated extensively [29–31]. Table I shows the results of numerical calculations performed by Martin [31] with $\gamma h/c \to \infty$, i.e. for a purely frictional material.

One potential approach for estimating q, λ, and κ for a ponderable material and any β is to draw on results from the kinematic method of limit analysis using a simple velocity field. This methodology, which applies to associated plastic flow, is discussed in detail by Chen [18]. An example of such a field is shown in Figure 4, and it closely resembles the Prandtl-type deformation field for weightless materials, where the difference lies in allowing angles ω_i $(i = 1, 2, 3, 4)$ to assume values resulting from minimization of q rather than from conditions imposed by the method of characteristics. A Hill-type deformation field could be considered in the same fashion. An attractive aspect of this approach is that κ is determined uniquely, since material velocities at the free surface are uniform by construction. If the velocity field were determined numerically using the method of characteristics, a representative value of κ (e.g. spatial average) would need to be evaluated to implement the approximate model. It should also be noted that a more sophisticated mechanism than the one in Figure 4, such as that considered by Michalowski [32] or Soubra [33], may lead to more accurate estimates of q, λ, and κ.

Table I. Values of N_γ, λ, and κ for $\beta = 0$ and Prandtl-type mechanism.

		Kinematic method (ponderable, cohesionless)			Equations (10) and (11) (weightless)	
ϕ (°)	Martin [31] N_γ	N_γ	λ	κ	λ	κ
0	0.00	0.00	—	—	1.00	0.50
10	0.43	0.77	0.45	3.98	1.57	0.79
20	2.84	4.58	1.10	3.88	2.53	1.26
30	14.75	21.70	2.21	5.32	4.29	2.14
40	85.57	120.0	4.42	9.11	8.01	4.01
50	742.9	1033.3	9.93	20.19	17.86	8.93

DOI: 10.1002/nag

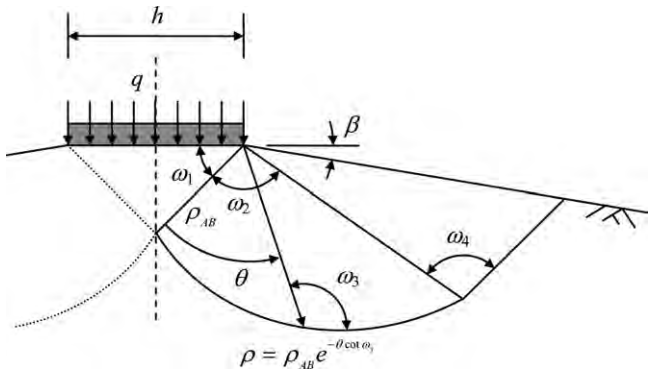

Figure 4. Prandtl-type mechanism used with kinematic method to estimate N_γ, λ, κ for ponderable, cohesionless material.

Table II. Values of N_γ, λ, and κ for $\beta>0$ using kinematic method with Prandtl-type mechanism.

		β/ϕ					
	ϕ (°)	0	0.1	0.2	0.3	0.4	0.5
$\frac{N_\gamma}{N_{\gamma,\beta=0}}$	10		0.96	0.92	0.88	0.84	0.80
	20		0.93	0.86	0.79	0.72	0.65
	30	1.00	0.88	0.77	0.67	0.57	0.49
	40		0.81	0.65	0.52	0.41	0.31
	50		0.71	0.50	0.35	0.24	0.17
$\frac{\lambda}{\lambda_{\beta=0}}$	10		1.07	1.15	1.25	1.37	1.53
	20		1.05	1.11	1.04	1.26	1.37
	30	1.00	1.03	1.06	1.09	1.14	1.20
	40		0.99	0.99	0.99	0.99	0.95
	50		0.95	0.90	0.86	0.72	0.60
$\frac{\kappa}{\kappa_{\beta=0}}$	10		0.93	0.85	0.78	0.71	0.64
	20		0.92	0.85	0.88	0.71	0.64
	30	1.00	0.91	0.83	0.75	0.68	0.61
	40		0.89	0.79	0.70	0.62	0.57
	50		0.85	0.72	0.61	0.57	0.56

Although the values of q, λ, and κ can be determined for materials with arbitrary ϕ, c, and γ, the case of $c=0$ (purely frictional material) is deemed the most interesting. For $\beta=0$, Table I shows values of N_γ appearing in the expression for calculating q (Equation (15)), as well as λ and κ, obtained using the kinematic method. Minimization was performed using the Levenberg–Marquardt optimization algorithm with a starting guess determined by a grid search over the range of admissible values of ω_i. Also presented in Table I are values of λ and κ for a weightless material. Clearly, predictions using the kinematic method indicate that more material is displaced over a smaller distance for a ponderable material as compared with a weightless material, and this agrees qualitatively with the solutions based on the method of characteristics [13]. Table II shows the variation in N_γ, λ, and κ with $\beta>0$, where tabulated values are normalized by the results for $\beta=0$.

Values of N_γ determined by Martin [31] are somewhat lower than those obtained using the kinematic method. Martin's values are closer to the true solution on account of their validity for both the partial stress field (lower bound) and velocity field (upper bound). Martin's values of N_γ were therefore used throughout this paper, and to account for the influence of $\beta>0$, these values were modified by the factor $N_\gamma/N_{\gamma,\beta=0}$ given in Table II.

DOI: 10.1002/nag

The kinematic method cannot be used for any flow rule other than an associated one, since dissipation along the discontinuities cannot be calculated. To account for $\psi<\phi$, it can be assumed that λ is the same as $\psi=\phi$, and that ψ only affects κ. This assumption is motivated by the behavior of κ with respect to ψ for weightless material and a non-coaxial flow rule (Equation (14)). Based on this assumption, κ is known at the extreme case $\psi=0$, which corresponds to incompressible material with $\kappa=1/(2\lambda)$. Values of κ for $0<\psi<\phi$ could be evaluated using an interpolating function possessing similar qualities as (14).

4. CYLINDER INDENTATION

This section is devoted to demonstrating the applicability of the approximate model to the case of cylinder indentation. Focus is restricted to a rough cylinder using the Prandtl-type punch solution, although it is also possible to consider a smooth cylinder by making use of the Hill-type punch solution.

The shape of a cylinder of radius r is given by the function

$$f(x)=r-\sqrt{r^2-x^2} \tag{16}$$

The contact length h, determined from (5), may be expressed through the following:

$$f(h/2)=r-\sqrt{r^2-\frac{h^2}{4}}=\delta+l, \quad h=2\sqrt{2r(\delta+l)-(\delta+l)^2} \tag{17}$$

Angle α is given by

$$f'(h/2)=\tan\alpha=\frac{h}{2\sqrt{r^2-(h/2)^2}} \tag{18}$$

Upon substituting (17) and (18) into (7), the differential equation governing the evolution of l as a function of δ becomes

$$\frac{\mathrm{d}l}{\mathrm{d}\delta}=\kappa-\frac{\kappa+1}{1+2\lambda\left[\dfrac{2r(\delta+l)-(\delta+l)^2}{l(r-\delta-l)}\right]} \tag{19}$$

No closed-form solution to Equation (19) could be found regardless of whether λ and κ are constant or varying. This equation was therefore solved numerically using initial conditions $l=l_0$, $\lambda=\lambda_0$, and $\kappa=\kappa_0$ at $\delta=0$. Equation (19) is singular with $l_0=0$, so l_0 was taken as a very small number in the numerical solution. For the cylinder, which has zero slope ($\tan\alpha=0$) at first contact with the material, it is reasonable to assume $\beta=0$ at $\delta=0$, and λ_0 and κ_0 are therefore determined using the relevant expressions from the previous section with $\beta=0$.

Equation (19) together with expressions for λ and κ (e.g. (10) and (11)) represent a coupled system of equations. The simple and robust numerical scheme used to solve this system is based on the Euler (forward) method. In this procedure, numerical values at the beginning of the finite difference step (δ_j, l_j, λ_j, and κ_j) were first used with Equation (19) to determine the value l_{j+1} corresponding to the end of the step, calculated based on the standard Euler method. Next, the value of β at the end of the increment (β_{j+1}) was calculated from Equation (1) using values of β and l at the end of the increment (δ_{j+1} and l_{j+1}) and the value of λ at the beginning of the increment (λ_j). Finally, new values λ_{j+1} and κ_{j+1} were determined using the suitable expressions for λ and κ based on the updated angle β_{j+1}. Since β_{j+1} is evaluated using λ_j, as opposed to λ_{j+1}, the method is fully explicit. A very small step size ($\Delta\lambda=\lambda_{j+1}-\lambda_j$) was used in all numerical calculations, with high fidelity of the results confirmed through a convergence study. In the case of ponderable material for which only numerical values of λ and κ are available (Tables I and II), cubic spline interpolation was used to arrive at functions that are continuous with respect to β.

DOI: 10.1002/nag

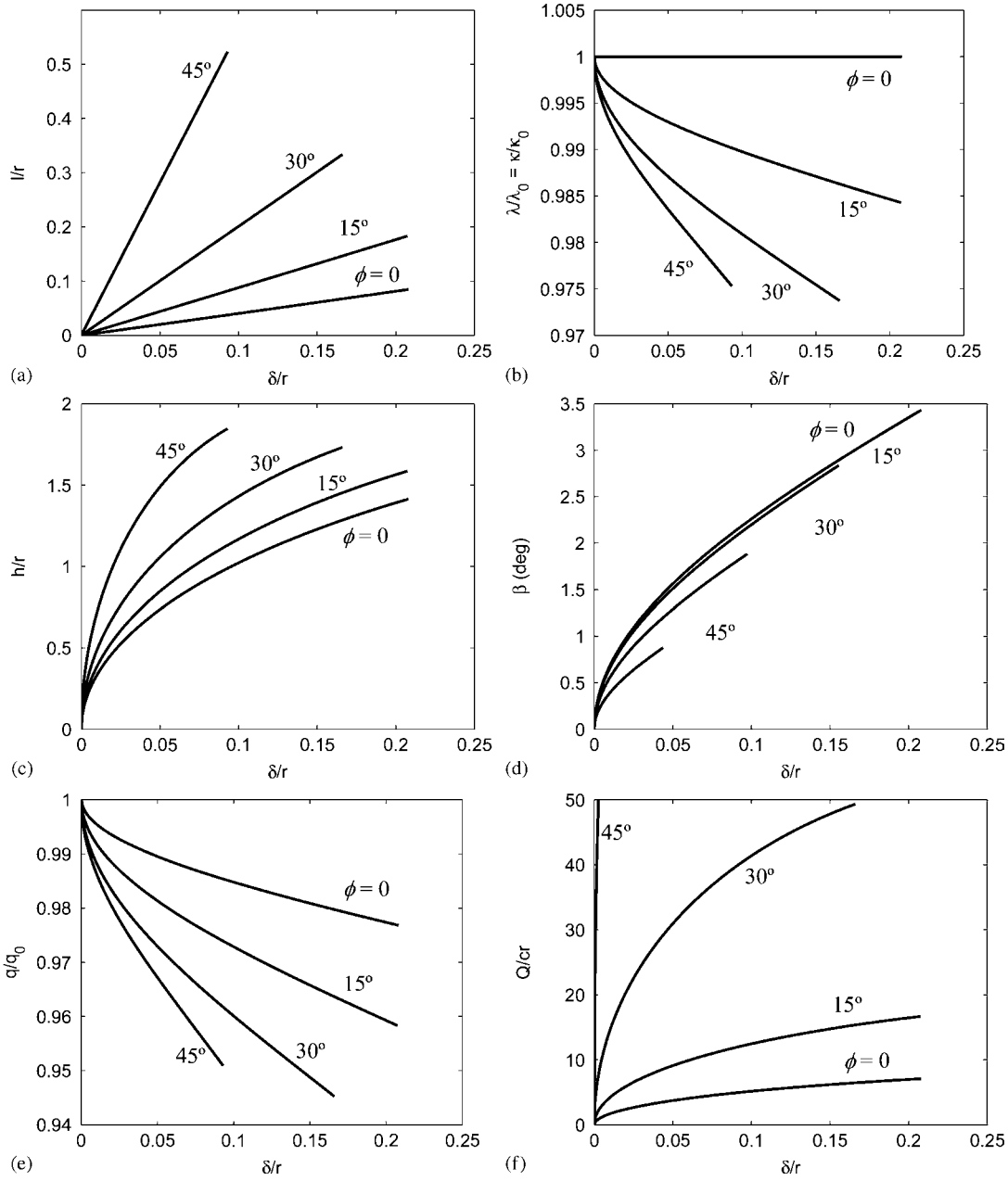

Figure 5. Numerical solution for cylinder indentation with weightless material obeying associated plastic flow: (a) normalized lip height l/r; (b) multipliers λ and κ; (c) normalized contact length h/r; (d) lip angle β; (e) average normal traction q; and (f) normalized total force Q/cr.

4.1. Weightless material

Figure 5 shows the numerical results for weightless material with associated plastic flow (Equations (9)–(11)). Although computations can be performed for relatively large values of δ/r, the Prandtl-type mechanism cannot be properly constructed for δ/r at which $\alpha > 45^\circ + \phi/2$, as the cylinder would lie partially outside the triangular region of material translating downward with the indenter. The solution is valid up to $\delta/r + l/r = 1 - \sqrt{2}/2 \approx 0.29$ for $\phi = 0$, with the bound on $\delta/r + l/r$ increasing as ϕ increases. Numerical results are plotted for δ/r ranging from zero to the limiting value.

DOI: 10.1002/nag

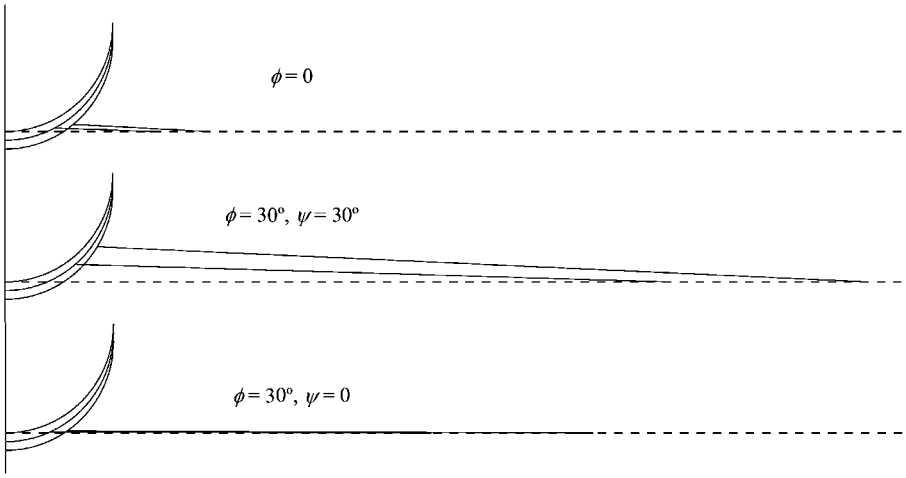

Figure 6. Deformed shape with weightless material and two values penetration, $\delta/r = 0.08$ and 0.16.

From Figure 5(a), it can be seen that normalized lip height l/r is nearly a linear function of normalized penetration δ/r for all ϕ. For given penetration, l/r increases dramatically with increasing ϕ as a result of growing dilatancy. Multipliers λ and κ (Figure 5(b)) decrease slightly throughout the indentation process but remain quite close to the initial values λ_0 and κ_0 ($\beta = 0$). For given penetration, h/r sharply increases and β slightly decreases with ϕ. Most importantly, β is always small ($\beta < 3.5°$), providing an *a posteriori* validation of the small-β approximation.

Much like h/r, normalized total force Q/cr (Figure 5(f)) increases with penetration at a decreasing rate. In fact, the variation in Q is primarily due to the changing contact length, since the average normal traction q (Figure 5(e)) decreases only slightly throughout the indentation process. In the figure, q is normalized by its initial value q_0, which corresponds to $\beta = 0$. For specified penetration, total force increases very sharply as a function of ϕ, due to an increase in both average normal traction and contact length.

Figure 6 shows the deformed shape for the cases $\phi = 0$ and $\phi = \psi = 30°$ at two particular values of normalized penetration. For $\phi = \psi = 30°$, the lips of displaced material are clearly very large in terms of both height (l) and length (λh). The large extent and volume of the material lips resulting from dilation in the case $\phi = \psi = 30°$ is not physically realistic.

Figure 7 shows the numerical results for $\phi = 30°$ and $\psi < \phi$, where κ is given by (14). The dilation angle ψ clearly has a profound effect on the predicted lip location and total force. When δ/r is fixed, the lip height l/r, contact length h/r, and normalized force Q/cr all increase substantially as ψ is increased. Again, q, λ, and κ remain close to the initial values. Lip angle β (not shown) is reduced significantly as ψ is varied from ϕ to 0.

The deformed shape for $\phi = 30°$ and $\psi = 0$ is also shown in Figure 6. In this case, material is displaced very thinly over a relatively large area, and the lip is barely perceptible without exaggeration in the vertical direction. Interestingly, lip height l is significantly smaller in the case of fully non-associated cohesive-frictional material ($\psi = 0$) than with cohesive material ($\phi = 0$). In both instances the material is incompressible, but material is displaced over a larger distance with than with $\phi = 0$.

It is acknowledged that the proposed model does not strictly conserve mass in the case of a cylinder and incompressible material. This can be seen by computing the total area of displaced material predicted using the proposed incremental formulation, which is somewhat less than the area occupied by the indenter below the undeformed surface. Nevertheless, this effect is small, and alternative schemes explored by the authors that strictly conserve mass predict similar overall results.

4.2. Ponderable material

Figure 8 plots key quantities from numerical computations for ponderable, cohesionless material with $\phi = 30°$. The basis for the calculations is the data tabulated in Tables I and II, as well as

DOI: 10.1002/nag

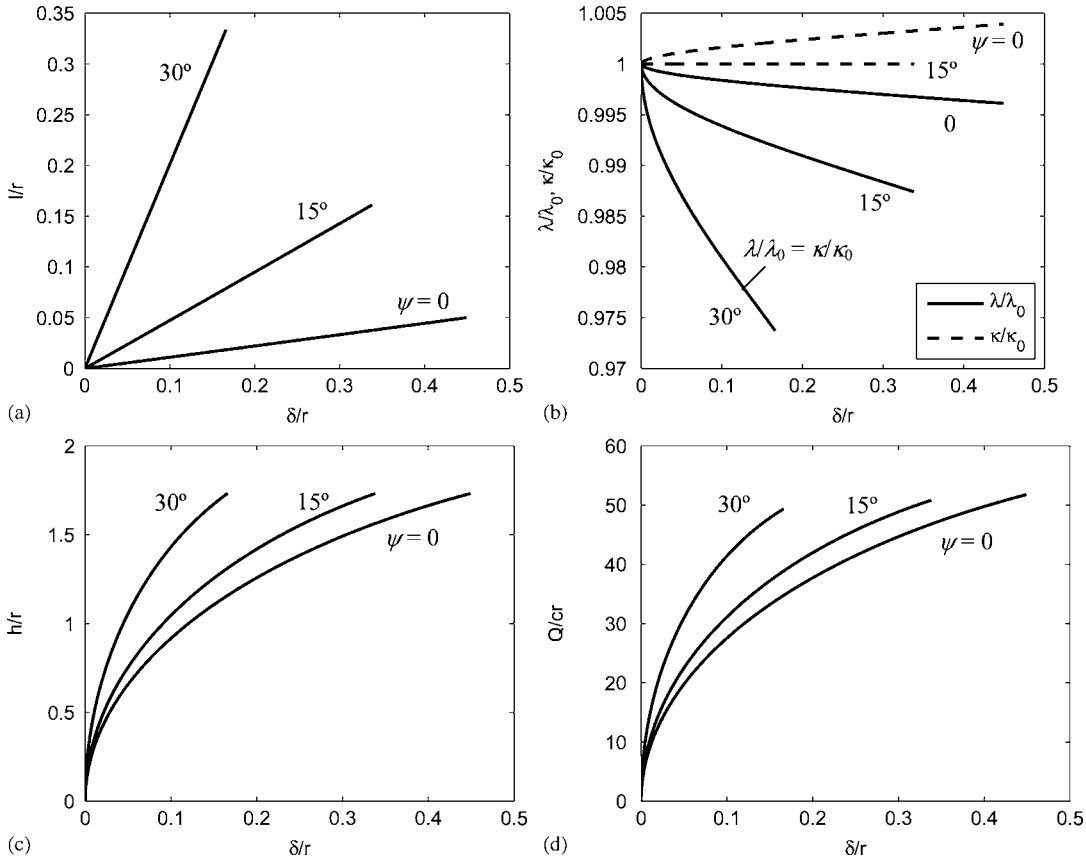

Figure 7. Numerical solution for cylinder indentation with weightless material ($\phi = 30^\circ$) and $\psi < \phi$: (a) normalized lip height l/r; (b) multipliers λ and κ; (c) normalized contact length h/r; and (d) normalized total force Q/cr.

Equation (15) with $c = 0$. Also shown in the figure for comparison are the results obtained for weightless material. As compared with weightless material, normalized lip height and contact length are significantly larger for ponderable material with $\phi = \psi$. This is ascribed to λ being smaller and κ being larger, so that more material is displaced over a smaller length λh with ponderable material. With $\phi = \psi$, multipliers λ and κ also undergo a larger variation during the indentation process compared with weightless material, where λ is increasing rather than decreasing. Lip angle β (not shown) also increases compared with weightless material as a result of the lip height l being larger and lip length λh being smaller.

Figure 8 also shows results for $\psi = 0$. These computations are based on using the same data for λ and N_γ as with $\psi = \phi$ but taking $\kappa = 1/(2\lambda)$, as discussed previously. From these results, we again find that ψ has great impact on the predicted lip location and total force, with l/r, h/r, and $Q/\gamma r^2$ dropping considerably as ψ is varied from ϕ to 0. For $\psi = 0$, the multipliers λ and κ, as well as the factor N_γ, change very little throughout the indentation process (Figure 8(b)) due to β remaining very small.

5. ASYMPTOTIC SOLUTION FOR CYLINDER

No exact solution to Equation (19) could be found, but in this section an approximate closed-form solution to Equation (19) is derived by examining the limiting (asymptotic) behavior at $\delta/r = 0$. This solution is obtained by rewriting (19) in dimensionless form and postulating a linear relationship between l/r and δ/r, motivated from linearity observed in the numerical results shown in Figures 5(a), 7(a), and 8(a). In particular, a solution of the form $l = \eta_{\text{asym}}\delta$ is considered, where η_{asym} is an

DOI: 10.1002/nag

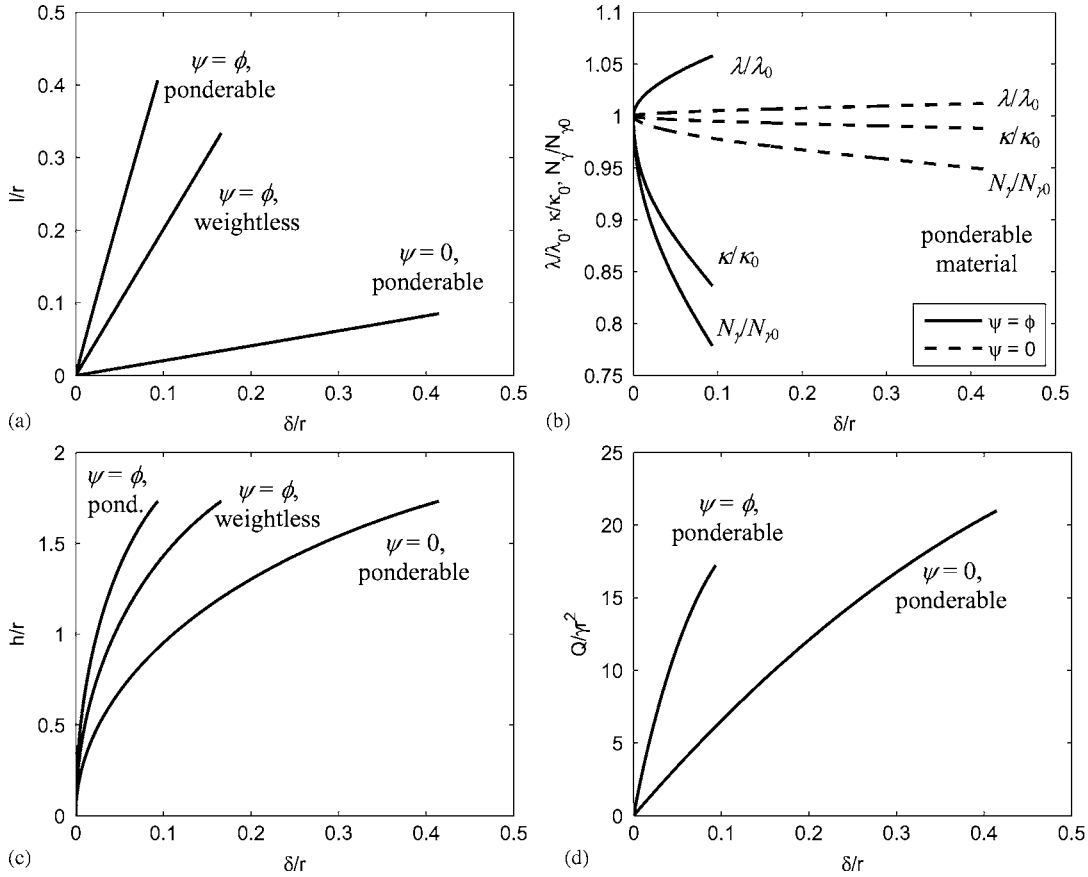

Figure 8. Numerical solution for cylinder indentation with ponderable material ($\phi = 30°$): (a) normalized lip height l/r; (b) factor N_γ and multipliers λ and κ; (c) normalized contact length h/r; and (d) normalized total force $Q/\gamma r^2$.

as yet unknown constant. Upon rewriting Equation (19) in terms of dimensionless variables and substituting $l = \eta_{\text{asym}}\delta$, the following expression is obtained:

$$\eta_{\text{asym}} = \kappa - \frac{\kappa + 1}{1 - 2\lambda\left[\dfrac{2(1+\eta_{\text{asym}}) - \dfrac{\delta}{r}(1+\eta_{\text{asym}})^2}{\eta_{\text{asym}}\left[\dfrac{\delta}{r}(1+\eta_{\text{asym}}) - 1\right]}\right]} \tag{20}$$

By taking $\delta/r = 0$, i.e. examining the asymptotic behavior corresponding to first contact, one arrives at an equation containing only constants η, λ, and κ, which may be solved to find

$$\frac{l}{\delta} = \eta_{\text{asym}} = \frac{4\lambda_0\kappa_0}{1 + 4\lambda_0} \tag{21}$$

Equation (21) is written in terms of λ_0 and κ_0 since λ and κ assume their initial values ($\beta = 0$) with $\delta/r = 0$.

The asymptotic solution given by (21) is remarkably simple. From this relation, the remaining quantities of interest, such as h and β (Equations (17) and (1)), are readily determined. In Figure 9, l/r and h/r from the asymptotic solution are compared with the numerical results for both weightless and ponderable material with $\phi = 30°$. The two sets of results are nearly indistinguishable when the material is weightless or incompressible ($\psi = 0$), and it is only for ponderable material with associated flow ($\psi = \phi$) that a slight difference is visible. Similar agreement was found for other values of ϕ.

DOI: 10.1002/nag

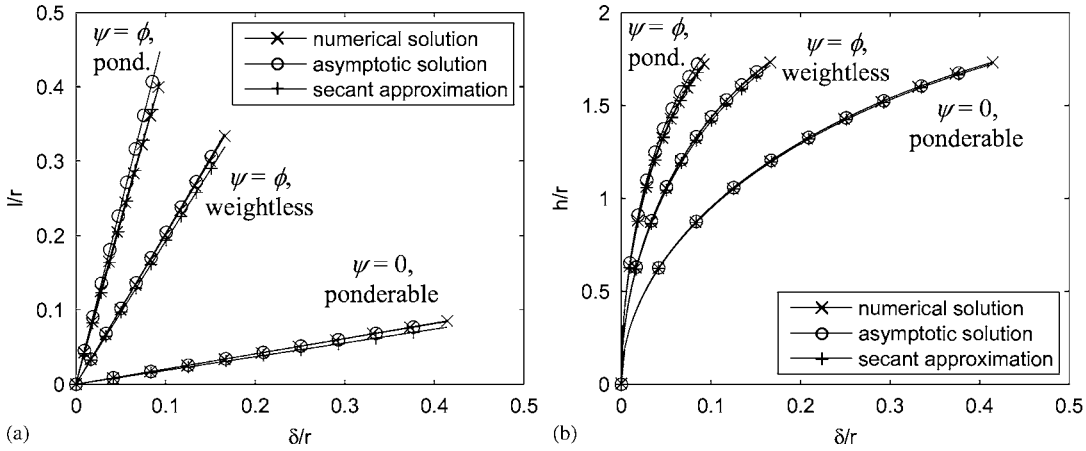

Figure 9. Numerical solutions, asymptotic solutions, and secant approximations for weightless material and associated plastic flow ($\phi = 30^\circ$): (a) normalized lip height l/r and (b) normalized contact length h/r.

Most importantly, analytic equations for total force Q that exhibit explicit dependence on δ may be easily obtained using (21). The expression for weightless material, for example, is

$$Q = 2c\cot\phi\sqrt{2r\delta(1+\eta_{\text{asym}})-\delta^2(1+\eta_{\text{asym}})^2} \times\left[\tan^2\left(\frac{\pi}{4}+\frac{\phi}{2}\right)\mathrm{e}^{\left(\pi-\frac{\eta_{\text{asym}}\delta}{\lambda_0\sqrt{2r\delta(1+\eta_{\text{asym}})-\delta^2(1+\eta_{\text{asym}})^2}}\right)\tan\phi}-1\right] \tag{22}$$

In (22), η_{asym} is given by (21), and λ_0 and κ_0 (in the expression for η_{asym}) are given by (10) and (14), respectively, with $\beta = 0$.

6. SECANT APPROXIMATION FOR ARBITRARY INDENTER SHAPE

In this section, an approximate analytic solution that holds for any blunt indenter is derived. This approximation rests on two key assumptions. The first is a secant approximation, $f'(x) \approx f(x)/x$, of the derivative appearing in Equation (7). By evaluating $f(x)$ and $f'(x)$ at $x = h/2$ (Equations (4) and (5)), the secant approximation gives

$$\tan\alpha = f'(h/2) \approx \frac{f(h/2)}{h/2} = 2\frac{\delta+l}{h} \tag{23}$$

From (23), it follows that the quantity $h\tan\alpha$ appearing in (7) is simply $2(\delta+l)$. As shown in Figure 10, the secant approximation is tantamount to replacing the curved indenter by an equivalent wedge, where the wedge's flanks pass through the indenter's lowermost point and the point of intersection of the indenter and material lip. As a consequence of the locally varying slope of the indenter, the equivalent wedge angle varies as a function of penetration δ.

The second assumption is that $\lambda = \bar{\lambda}$ and $\kappa = \bar{\kappa}$, where $\bar{\lambda}$ and $\bar{\kappa}$ are constants that may in general be different from λ_0 and κ_0. The validity of taking λ and κ to be constant is supported by numerical results for the cylinder, which show that λ and κ do not deviate substantially from their initial values. Also, an intrinsic part of the asymptotic solution discussed in the previous section is that λ and κ are constants, and this solution was in close agreement with numerical results for the cylinder.

DOI: 10.1002/nag

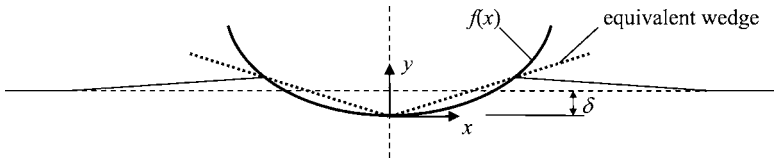

Figure 10. Replacement of curved indenter by equivalent wedge through secant approximation.

Upon substitution of (23) into (7) with $\lambda=\bar{\lambda}$ and $\kappa=\bar{\kappa}$, the governing equation becomes

$$\frac{\mathrm{d}l}{\mathrm{d}\delta}=\bar{\kappa}-\frac{\bar{\kappa}+1}{2\bar{\lambda}\left(\frac{\delta}{l}+1\right)+1} \tag{24}$$

Like the asymptotic solution, Equation (24) has a solution of linear form $l=\eta\delta$, where η is a constant. Substitution of $l=\eta\delta$ into Equation (24) provides an equation that may be solved to find

$$\frac{l}{\delta}=\eta=\frac{2\bar{\lambda}\bar{\kappa}}{1+2\bar{\lambda}} \tag{25}$$

The approximate solution (25) applying to arbitrary indenter geometry is similar to the asymptotic solution for the cylinder (Equation (21)), where only the coefficients are different. The solution obtained based on the secant approximation using $\bar{\lambda}=\lambda_0$ and $\bar{\kappa}=\kappa_0$ is also shown in Figure 9, with the curves falling slightly slower than those based on the asymptotic solution but again being very close to the numerical results.

It may be noted that (25) can also be obtained for arbitrary $f(x)$ using a first-order Taylor approximation $f(x)\approx f'(0)x$. For a cylinder, however, one finds $f'(0)=0$, and the interpretation of a result like (25) would be ambiguous. For the cylinder, a second-order approximation $f(x)\approx \frac{1}{2}f''(0)x^2$ is required to derive an analytic solution, and in this case, the asymptotic solution (Equation (21)) is recovered.

7. BLUNT WEDGE INDENTATION

In this section, the approximate model is applied to wedge indentation. Again, only the Prandtl-type mechanism (rough wedge) is considered, although solutions for a Hill-type mechanism can also be obtained. With its shape given by $f(x)=x\tan\alpha$ (α constant), the wedge is the simplest type of indenter. The solution using the secant approximation (Equation (25)) is exact for the wedge, and one readily finds

$$l=\eta\delta \tag{26}$$

$$h=2\delta\cot\alpha(1+\eta) \tag{27}$$

$$\beta=\frac{\eta\tan\alpha}{2\bar{\lambda}(1+\eta)} \tag{28}$$

where $\eta=2\bar{\lambda}\bar{\kappa}/(1+2\bar{\lambda})$.

7.1. Weightless material

Constants $\bar{\lambda}$ and $\bar{\kappa}$ are determined by solving Equations (10) and (14) after making the substitutions $\lambda=\bar{\lambda}$ and $\kappa=\bar{\kappa}$. A numerical method is required to obtain exact values of $\bar{\lambda}$ and $\bar{\kappa}$ for particular

DOI: 10.1002/nag

Table III. Values of l/δ, h/δ, β, and $Q/\delta c$ for wedge indentation with weightless material.

					$Q/\delta c$	
	α (°)	$\frac{l}{\delta}$	$\frac{h}{\delta}$	β (°)	Equation (31)	Tordesillas and Shi [12]
$\phi=0$	10	0.333	15.12	1.26	77.092	77.095
	20		7.33	2.61	37.004	37.010
	30		4.62	4.13	23.081	23.090
	40		3.18	6.01	15.673	15.685
$\phi=30°$, $\psi=30°$	10	1.92	33.13	0.77	982.2	976.6
	20		16.05	1.60	467.5	462.0
	30		10.12	2.54	288.9	283.4
	40		6.96	3.69	194.0	188.6
$\phi=30°$, $\psi=0$	10	0.104	12.53	0.11	376.65	376.69
	20		6.07	0.23	182.01	182.04
	30		3.83	0.36	114.41	114.44
	40		2.63	0.53	78.45	78.47

values of α and ϕ, since β depends on $\bar{\lambda}$ and $\bar{\kappa}$ according to Equation (28). However, explicit expressions may be obtained by neglecting β in (10) and (14), in which case $\bar{\lambda}$ and $\bar{\kappa}$ are

$$\bar{\lambda}\approx\lambda_0=\tan\left(\frac{\pi}{4}+\frac{\phi}{2}\right)e^{\frac{\pi}{2}\tan\phi},\quad \bar{\kappa}\approx\kappa_0=\frac{1}{2}\frac{\cos\phi\cos\left(\frac{\pi}{4}+\frac{\phi}{2}-\psi\right)}{[\cos(\phi-\psi)-\sin\psi]\sin\left(\frac{\pi}{4}+\frac{\phi}{2}\right)}e^{-\frac{\pi}{2}\tan(\phi-2\psi)} \tag{29}$$

Exact values of $\bar{\lambda}$ and $\bar{\kappa}$ calculated for $0<\alpha\leqslant 40°$ and $0\leqslant\phi\leqslant 50°$ differ by less than 4% as compared with the approximate values obtained with Equation (29). Using $\bar{\lambda}=\lambda_0$ and $\bar{\kappa}=\kappa_0$, it follows that

$$\eta=\frac{\tan\left(\frac{\pi}{4}+\frac{\phi}{2}\right)e^{\frac{\pi}{2}\tan\phi}}{1+2\tan\left(\frac{\pi}{4}+\frac{\phi}{2}\right)e^{\frac{\pi}{2}\tan\phi}}\frac{\cos\phi\cos\left(\frac{\pi}{4}+\frac{\phi}{2}-\psi\right)}{\left[\cos(\phi-\psi)-\sin\psi\right]\sin\left(\frac{\pi}{4}+\frac{\phi}{2}\right)}e^{-\frac{\pi}{2}\tan(\phi-2\psi)} \tag{30}$$

Expressions for l, h, and β may be obtained from (26)–(28), and evaluating $Q=qh$ using the formula for q from (9) gives the following expression for total force:

$$Q=\frac{2\delta c(1+\eta)}{\tan\phi\tan\alpha}\left[\tan^2\left(\frac{\pi}{4}+\frac{\phi}{2}\right)e^{\left(\pi-\frac{\eta\tan\alpha}{\lambda_0(1+\eta)}\right)\tan\phi}-1\right] \tag{31}$$

In (31), λ_0 and η are taken from (29) and (30), respectively.

In Table III, predictions of $Q/\delta c$ from Equation (31) are compared with values calculated numerically using the implicit formulas of Tordesillas and Shi [12], which in the case $\phi=0$ are identical to formulas obtained earlier by Haddow [10]. The solutions agree very well, with small differences apparently arising due to the approximations $\sin\beta\approx\beta$, $\bar{\lambda}\approx\lambda_0$, and $\bar{\kappa}\approx\kappa_0$.

From Table III, it is seen that lip height and contact length at a given penetration are strongly dependent on ϕ and ψ, much like in cylinder indentation. Most significantly, an increase in dilatancy causes the lip height and contact length to become larger, which in turn requires an increase in total force.

7.2. Ponderable material

Expressions of l, h, and β, and Q for ponderable material may be derived in the same way as with weightless material, with numerical data (Tables I and II) available for determining $\bar{\lambda}$ and $\bar{\kappa}$. The

DOI: 10.1002/nag

Table IV. Values of l/δ, h/δ, β, and $Q/\delta c$ for wedge indentation with ponderable, cohesionless material.

	α (°)	$\frac{l}{\delta}$	$\frac{h}{\delta}$	β (°)	$Q/\delta^2\gamma$
$\phi=30°$, $\psi=30°$	10	4.33	60.49	1.86	24955
	20		29.31	3.84	5370
	30		18.47	6.09	1930
	40		12.71	8.85	805
$\phi=30°$, $\psi=0$	10	0.185	13.44	0.36	1312
	20		6.51	0.74	303
	30		4.10	1.17	118
	40		2.82	1.70	54.8

simplifying assumption $\bar{\lambda}=\lambda_0$ and $\bar{\kappa}=\kappa_0$ is introduced from the outset. Combining Equations (15) and (27), the total force for cohesionless material is given by

$$Q=2\delta^2\gamma\cot^2\alpha\left(1+\frac{2\lambda_0\kappa_0}{1+2\lambda_0}\right)^2 N_\gamma \tag{32}$$

For $\psi=\phi$, constants λ_0, κ_0, and N_γ in (32) are determined using Tables I and II, where N_γ is evaluated by interpolating data in Table II with the appropriate value of β (Equation (28)). In the case $\psi=0$, λ_0 and N_γ are again taken directly from Tables I and II, except that κ is given by $\kappa=1/(2\lambda)$.

Table IV shows normalized lip height, contact length, and total force for ponderable, cohesionless material with $\phi=30°$ and the two cases $\psi=30°$ and $\psi=0$. As compared with weightless material, lip height and contact length are much larger with ponderable material due to more material being displaced over a smaller area next to the wedge. Also, dilatancy has a drastic affect on the lip location and total force. For example, normalized force $Q/\delta^2\gamma$ with $\psi=30°$ is nearly 20 times that with $\psi=0$ for $\alpha=10°$.

8. FEM SIMULATION

To assess the validity of the approximate model presented, FEM simulations using the code ABAQUS/Explicit were performed. This program is based on explicit time integration of the equations of dynamic equilibrium, a scheme that is very efficient for problems involving large, plastic deformation. The FEM simulations were similar to those described in an earlier paper dealing with wheel indentation [17]. An elastic-plastic constitutive law based on the Drucker–Prager yield condition and a corresponding associated or non-associated flow potential was used, for which parameters can be chosen to closely match the Mohr–Coulomb model [34]. The constitutive law used was therefore based on coaxial plastic flow, although results from the analytic model developed for non-coaxial flow are still used in comparison. A large value of Young's modulus E was specified to emulate rigid-plastic behavior (e.g. $E/c\approx 7000$ for $\phi=0$), and Poisson's ratio was taken as $\nu=0.3$.

FEM simulation consisted of first applying unit weight, if present, to a finite, rectangular domain of material and then displacing the indenter into the material until the contact length reached a specified value, denoted h^*. The domain was made large enough so that conditions on the boundaries other than the free surface had minimal effect on the results. During displacement of the indenter, the arbitrary Lagrangian–Eulerian (ALE) remeshing algorithm available in the code was utilized in the region of material near the indenter to maintain a high-quality mesh. Contact interactions between the indenter and material were enforced using the kinematic contact algorithm available in the code. Contact conditions consisted of dry friction μ and maximum shear stress $\tau_{\max}=c$ for cohesive materials and dry friction $\mu=\tan\phi$ without a maximum shear stress for cohesive-frictional material.

DOI: 10.1002/nag

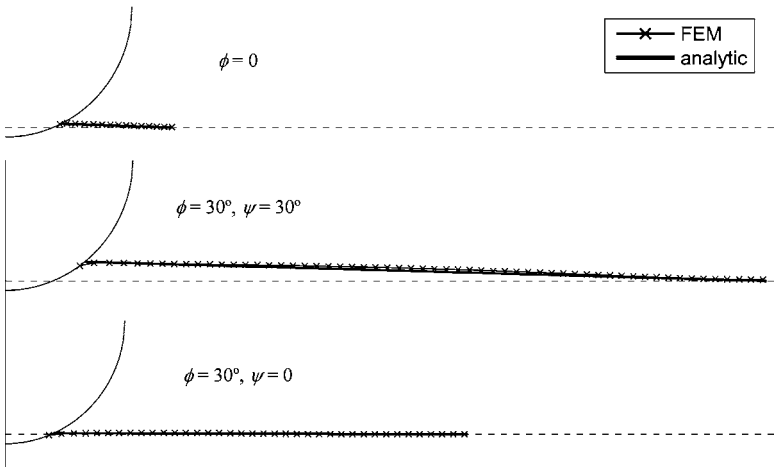

Figure 11. Comparison of free surfaces from FEM simulation and approximate model for weightless material ($\delta/r = 0.07$).

Accurate time integration was achieved by simulating the process over a period of time that was sufficiently large for quasi-static conditions to apply. A mesh refinement study also showed that errors due to spatial discretization were small (i.e. less than 2%) using linear quadrilateral reduced-integration elements with $L_e/h^* \approx 0.02$, where L_e is the edge length of the initially square elements near the indenter.

Figure 11 compares the lip locations determined using FEM simulation with those from approximate model for weightless material. For cohesive material, excellent agreement can be seen, with the lip height from the approximate model being only slightly less than that from FEM simulation. For cohesive-frictional material with $\psi = \phi$ and $\psi = 0$, the agreement is also very good, where FEM results show that material is displaced thinly over a relatively large distance with $\psi = 0$. Although the lip geometries from FEM simulation are not straight and differ on a point-wise basis from the lip geometry from the approximate model, the overall deformed shape is predicted very well using the approximate model. In particular, predictions of lip height and contact length are close to the values from FEM simulation.

As shown in Figure 12, the lip location for ponderable material is also predicted very well using the approximate model. In the FEM simulations, the material was nearly cohesionless, with small cohesion ($c/\gamma r = 0.17$) included to provide stability. Agreement between analytic and FEM results provides a validation of the values of λ and κ for ponderable material from Tables I and II, which were estimated using the kinematic method of limit analysis.

As shown in Figures 13 and 14, the force–penetration relationships from the approximate approach and FEM simulation also agree very well. In the case of weightless cohesive material ($\phi = 0$) and cohesive-frictional material with $\phi = \psi$, the agreement is excellent. For $\psi = 0$, the force–penetration curve from FEM simulation lies below the curve from the approximate model when q (Equation (9)) is evaluated using the true material properties ϕ and c. Estimating q based on the modified constants ϕ^* and c^* (Equations (12) and (13)) brings the curve closer to the FEM results for weightless material, as shown by the dashed line in Figure 13. With ponderable, nearly cohesionless material (Figure 14), for which there is greater uncertainty in accurately assessing λ, κ, and q, the results obtained with true constants ϕ and c are nearer to the FEM predictions than with ϕ^* and c^*.

9. DISCUSSION OF RESULTS

In the approximate model, quantities q, λ, and κ depend on lip angle β and are assessed from the analogous problem involving a flat rigid punch pressed into a surface that slopes at angle β (truncated wedge). For the cylinder and wedge, respectively, Figures 15 and 16 show predicted

DOI: 10.1002/nag

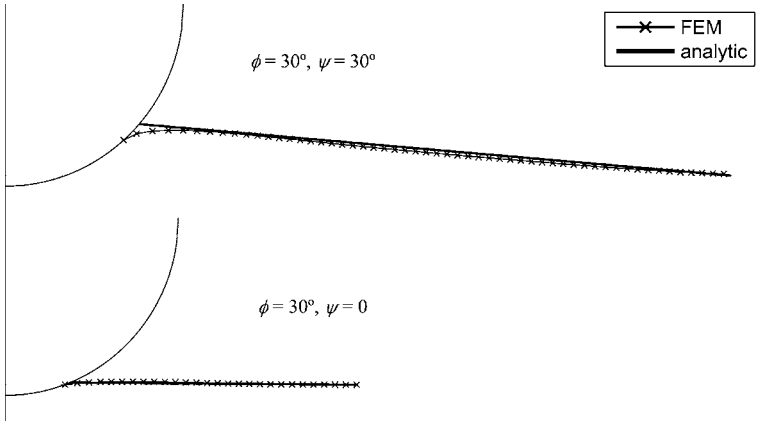

Figure 12. Comparison of free surfaces from FEM simulation and approximate model for ponderable material ($\delta/r = 0.06$).

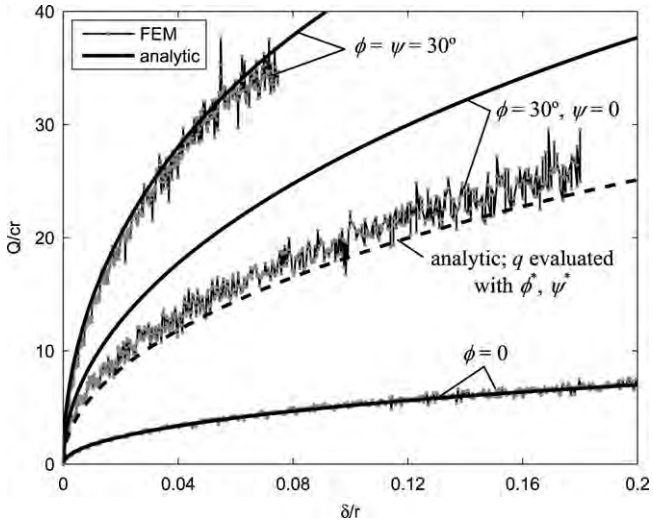

Figure 13. Comparison of force–penetration curves from FEM simulation and approximate model for cylinder on weightless material.

force–penetration relationships that were obtained from numerical computations based on evaluating q, λ, and κ with $\beta \neq 0$. Also shown are the results obtained when q, λ, and κ are evaluated by taking $\beta = 0$ in the relevant expressions (e.g. Equations (9)–(11)). The two approaches ($\beta \neq 0$ and $\beta = 0$) clearly yield similar results, with a substantial discrepancy appearing only in the case of ponderable material with $\psi = \phi$.

A major ramification of the viability of evaluating q, λ, and κ with $\beta = 0$ is that the solution for an indentation process may be constructed with reasonable accuracy based simply on results for a rigid punch pressed into a flat surface. In other words, satisfactory results may be achieved without knowing the solution to the truncated wedge problem, which is considerably less tractable than when the surface is flat, especially when the material's weight is included. It should be recognized that while q, λ, and κ may be taken as constants corresponding to $\beta = 0$, the lips of displaced material with inclination $\beta \neq 0$ remain present in the approximate model.

In the approximate model, major emphasis is placed on predicting the evolving geometry of material displaced by the indenter, especially with regard to evolution of contact length. The effect of displaced material on indentation force can be illustrated by considering the results obtained when displaced material is altogether neglected (i.e. $l = \beta = 0$) and contact length is therefore taken

DOI: 10.1002/nag

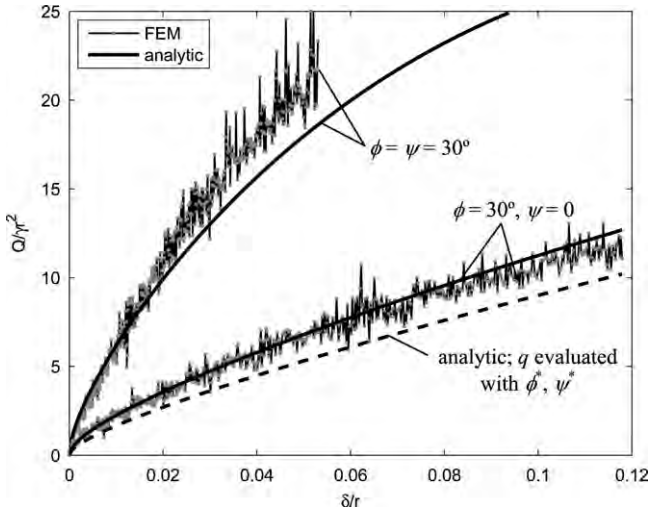

Figure 14. Comparison of force–penetration curves from FEM simulation and approximate model for cylinder on ponderable material with small cohesion ($c/\gamma r = 0.17$).

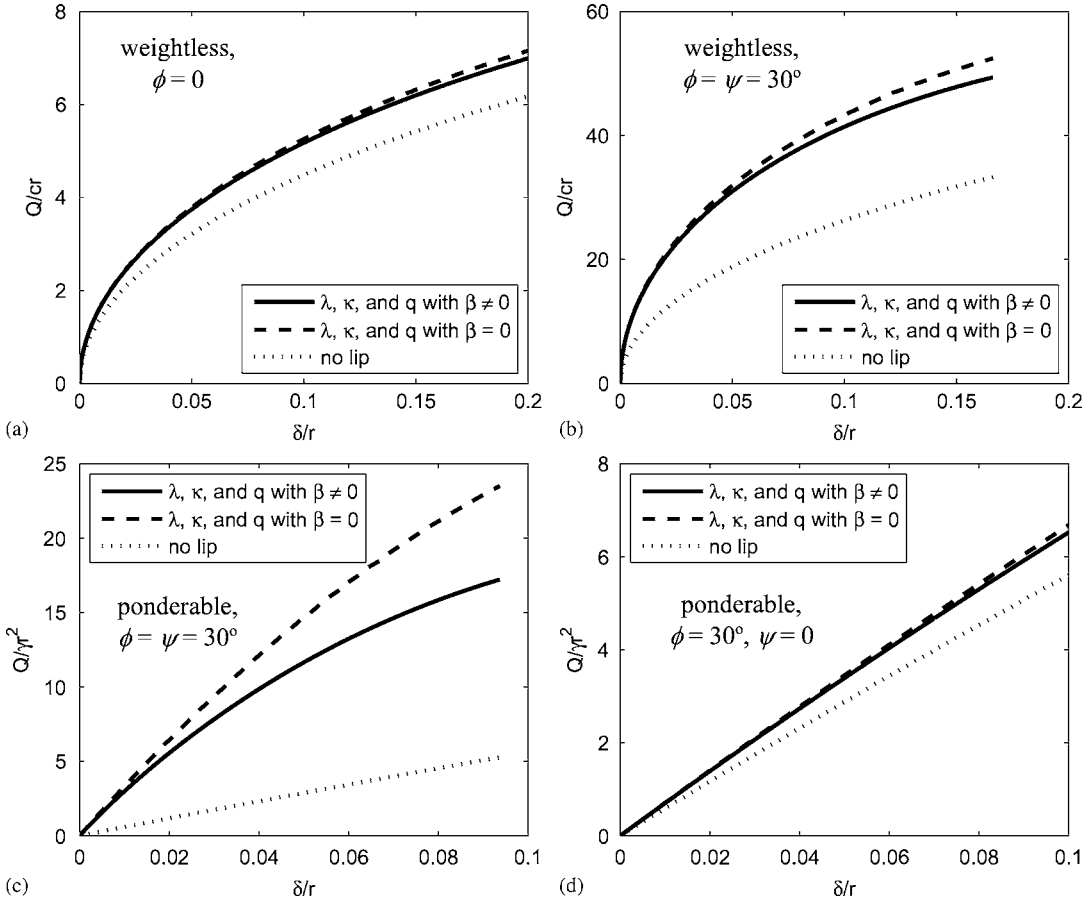

Figure 15. Exact force–penetration relationships for cylinder compared with zero-β and no-lip approximations.

DOI: 10.1002/nag

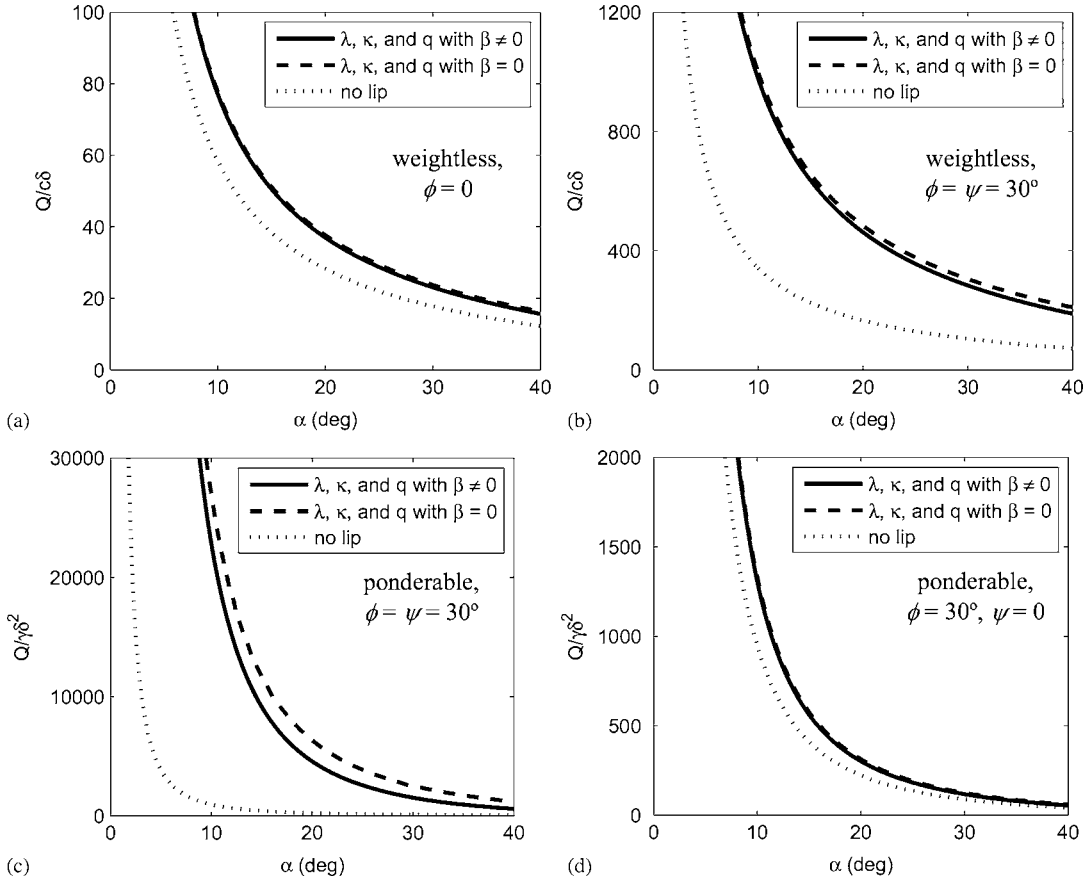

Figure 16. Exact force computations for wedge compared with zero-β and no-lip approximations.

as the length over which the indenter intersects the undisturbed material surface. These results are also shown in Figures 15 and 16. In contrast with the small error introduced by approximating q, λ, and κ as constants corresponding to $\beta = 0$ (dashed lines), neglecting displaced material and therefore underestimating contact length leads to a large error (dotted lines). Furthermore, displaced material has a particularly profound effect on the indentation force for dilating material (Figures 15(b), (c) and 16(b), (c)). For the wedge (Figure 16), the influence of displaced material becomes very large as the angle α of the wedge flank becomes small (i.e. the wedge semi-angle becomes large). With small α, a small variation in lip height has a tremendous effect on contact length.

10. CONCLUSIONS

This paper presents an approximate model for the process of a blunt object indenting rigid-plastic material, where special consideration is given to the evolving contact at the indenter-material interface and boundary geometry. This model is based on approximating the lips of displaced material adjacent to the indenter as straight and determining the lip location (i.e. lip height l and angle β) from an evolution equation (Equation (7)) derived from kinematical considerations for an increment of deformation. The model further assumes that an increment of deformation is analogous to that of a flat rigid punch pressed into a surface that is inclined at angle β on either side of the punch (truncated wedge). Since the punch problem is relatively well understood, the proposed model yields results for a wide variety of materials, including ponderable materials. By introducing several simplifying assumptions in the approximate model, accurate analytic expressions relating

DOI: 10.1002/nag

lip height l, lip angle β, contact length h, average normal traction q, and ultimately indentation force Q to penetration δ are available. Cylindrical and wedge-shaped indenters were investigated in detail in the paper, although the model may be applied to arbitrary indenter shape provided the ratio δ/h remains small (i.e. blunt indenter).

The approximate model relies on utilizing three key quantities from the problem of a flat rigid punch resting on a surface: λ, κ, and q. The quantity λ may be viewed as the normalized lip length, while κ is dimensionless normal velocity (or flux) at points along the lip surface. For all materials considered in this paper, λ was found to be independent of dilatancy, whereas κ depended on the dilation angle ψ. For weightless materials, the quantities λ, κ, and q may be precisely determined from classical solutions to the problem involving a flat punch. For ponderable materials, quantities λ, κ, and q can be evaluated tractably using the kinematic method of limit analysis.

A finding seen as having paramount significance in the process of blunt object indentation is that information from the problem of a flat rigid punch resting on a $flat$ surface is sufficient to construct the force–penetration relationship for an indentation process with reasonable accuracy. In particular, quantities λ, κ, and q can be taken as constants and estimated from the punch problem with $\beta = 0$. The problem involving a flat punch on a flat surface can in this way be regarded as fundamental, in much the same way as the Flamant solution is a fundamental solution in linear elastic theory.

The presence of the lips of displaced material adjacent to the indenter was found to have a significant influence on the indentation force. This is especially true for dilating materials, for which a potentially large error would be introduced by disregarding material displaced by the indenter. The error introduced by neglecting displaced material comes from underestimation of the contact length, which is the single most important factor in determining total force. Displaced material has a particularly large influence on indentation force for blunt indenters, as a small increase in height of the material lips causes a relatively large increase in the contact length.

For the cylinder, very good agreement between the approximate analytic predictions and results from FEM simulations was demonstrated. For the wedge, the approximate model provides a synthesized framework for understanding problems that have been considered separately in the literature [7–10, 12] and generates novel explicit analytic formulae that agree with the implicit equations obtained by other authors. Compared with previous works, a key assumption that enables explicit analytic formulae to be determined is that angle β is small. This small-angle approximation was validated *a posteriori* in this paper.

Some degree of interface friction is present in any real indentation process. Accordingly, emphasis was placed on rough indenters in this paper. For blunt indenters, the value of friction needed for a dead material cap to form beneath the indenter can be quite low [9, 12], and the pattern of deformation will be of the Prandtl-type shown in Figure 3. Nevertheless, the model also applies to smooth indenters. In order to apply λ, κ, and q from the punch problem to smooth indenters possessing curvature, an implicit assumption is that the curved surface can be approximated as flat as required, but such an assumption seems reasonable when the indenter is blunt.

Findings in this paper pertain to rigid-perfectly plastic materials for which elastic effects are secondary. Such materials include clays, dense sands, and some soft metals. Validation of the proposed theoretical model via experiments remains an item of future work, as published experimental results are for sharp wedges [13, 15] and narrow cylinders, or wheels [17].

Using an approach similar to the one presented in this paper, force–penetration relationships may also be developed for axisymmetric (e.g. sphere, cone, etc.) or other three-dimensional indenters (e.g. pyramid, cylinder of finite length, etc.). Such analyses would be based, for instance, on parameters identified from the axially symmetric punch problem [35] or the three-dimensional problem for a generally rectangular punch [36].

DOI: 10.1002/nag

ACKNOWLEDGEMENTS

Financial support provided by the Shimizu Corporation is gratefully acknowledged. Computer resources were provided by the Minnesota Supercomputing Institute.

REFERENCES

1. Johnson KL. *Contact Mechanics*. Cambridge University Press: Cambridge, 1985.
2. Schnaid F. *In Situ Testing in Geomechanics*: *The Main Tests*. Taylor & Francis: London, 2009.
3. Bekker MG. *Introduction to Terrain-Vehicle Systems*. University of Michigan Press: Ann Arbor, 1969.
4. Shen J, Kushwaha RL. *Soil–Machine Interactions*: *A Finite Element Perspective*. Marcel Dekker, Inc.: New York, 1998.
5. Hill R. *The Mathematical Theory of Plasticity*. Oxford University Press: Oxford, 1950.
6. Petryk H. Non-unique slip-line field solutions for the wedge indentation problem. *Journal de Mécanique Appliqué* 1980; **4**(3):255–282.
7. Hill R, Lee EH, Tupper SJ. Theory of wedge indentation of ductile materials. *Proceedings of the Royal Society of London*, *Series A*: *Mathematical*, *Physical and Engineering Sciences* 1947; **188**(1013):273–289.
8. Shield RT. Mixed boundary value problems in soil mechanics. *Quarterly of Applied Mathematics* 1953; **11**(1): 61–75.
9. Grunzweig J, Longman IM, Petch NJ. Calculations and measurements on wedge-indentation. *Journal of Mechanics and Physics of Solids* 1954; **2**(2):81–86.
10. Haddow JB. On a plane strain wedge indentation paradox. *International Journal of Mechanical Sciences* 1967; **9**(4):159–161.
11. Bai Y, Dodd B. Slip-line field solution for plane-strain indentation by an obtuse-angle wedge. *International Journal of Mechanical Sciences* 1982; **24**(2):119–123.
12. Tordesillas A, Shi J. Frictional indentation of dilatant granular materials. *Proceedings of the Royal Society of London*, *Series A*: *Mathematical*, *Physical and Engineering Sciences* 1999; **455**(1981):261–283.
13. Drescher A, Kwaszczynska K, Mróz Z. Statics and kinematics of granular medium in case of wedge indentation. *Archiwum Mechaniki Stosowanej* 1967; **19**(1):99–113.
14. Drescher A, Michalowski RL. Density variation in pseudo-steady plastic flow of granular media. *Géotechnique* 1984; **34**(1):1–10.
15. Butterfield R, Andrawes KZ. An investigation of a plane strain continuous penetration problem. *Géotechnique* 1972; **22**(4):597–617.
16. Butterfield R. The kinematics of self-similar plane penetration problems in Mohr–Coulomb granular materials. In *Rock and Soil Rheology*, Bhattacharji S, Friedman GM, Neugebauer HJ, Seilacher A (eds). vol. 14. Springer: Berlin, 1988; 83–92.
17. Hambleton JP, Drescher A. Modeling wheel-induced rutting in soils: indentation. *Journal of Terramechanics* 2008; **45**(6):201–211.
18. Chen WF. *Limit Analysis and Soil Plasticity*. Elsevier: Amsterdam, 1975.
19. Mróz Z, Szymański C. Non-associated flow rules in description of plastic flow of granular materials. In *Limit Analysis and Rheological Approach in Soil Mechanics*, Olszak W, Šuklje L (eds). Springer: New York, 1978; 51–94.
20. Vermeer PA, de Borst R. Non-associated plasticity for soils, concrete and rock. *Heron* 1984; **29**(3):1–62.
21. de Borst R, Vermeer A. Possibilities and limitations of finite elements for limit analysis. *Géotechnique* 1984 **34**(2):199–210.
22. Cox AD. The use of non-associated flow rules in soil plasticity. *Royal Armament Research and Development Establishment*, *Report B*, 2/63, 1963.
23. Drescher A, Detournay E. Limit load in translational failure mechanisms for associative and non-associative materials. *Géotechnique* 1993; **43**(3):443–456.
24. de Josselin de Jong G. Statics and kinematics in the failable zone of a granular material. *Doctoral Thesis*, Delft University, 1959.
25. Spencer AJM. Theory of kinematics of ideal soils under plane strain conditions. *Journal of Mechanics and Physics of Solids* 1964; **12**(5):337–351.
26. Mehrabadi MM, Cowin SC. Initial planar deformation of dilatant granular materials. *Journal of the Mechanics and Physics of Solids* 1978; **26**(4):269–284.
27. Sokolovskii VV. *Statics of Granular Media*. Pergamon: Oxford, 1965.
28. Terzaghi K. *Theoretical Soil Mechanics*. Wiley: New York, 1943.
29. Michalowski RL. An estimate of the influence of soil weight on bearing capacity using limit analysis. *Soils and Foundations* 1997; **37**(4):57–64.
30. Ukritchon B, Whittle AJ, Klangvijit C. Calculations of bearing capacity factor N using numerical limit analyses. *Journal of Geotechnical and Geoenvironmental Engineering* 2003; **129**(5):468–474.
31. Martin CM. Exact bearing capacity calculations using the method of characteristics. *Proceedings of the 11th International Conference of IACMAG*, Turin, Italy, 19–24 June 2005; 441–450.

DOI: 10.1002/nag

32. Michalowski RL. An estimate of the influence of soil weight on bearing capacity using limit analysis. *Soils and Foundations* 1997; **37**(4):57–64.
33. Soubra A-H. Upper-bound solutions for bearing capacity of foundations. *Journal of Geotechnical and Geoenvironmental Engineering* 1999; **125**(1):59–68.
34. ABAQUS Version 6.6 Documentation. ABAQUS, Inc., Providence, 2006.
35. Cox AD, Eason G, Hopkins HG. axially symmetric plastic deformations in soils. *Philosophical Transactions of the Royal Society A* 1961; **254**(1036):1–45.
36. Michalowski RL. Upper-bound load estimates on square and rectangular footings. *Géotechnique* 2001; **51**(9): 787–798.

DOI: 10.1002/nag